

ANALYSIS METHODS FOR ELECTRON RADIOGRAPHY BASED ON LASER-PLASMA ACCELERATORS*

G. Bruhaug[†], G. W. Collins, H. G. Rinderknecht, J. R. Rygg, J. L. Shaw, M. S. Wei
 Laboratory for Laser Energetics, University of Rochester, Rochester, NY, USA
 M. S. Freeman, F. E. Merrill, L. P. Neukirch, C. H. Wilde
 Los Alamos National Laboratory, Los Alamos, NM, USA

Abstract

Analysis methods are presented for determining the resolution of both contact and projected electron radiography based on a laser-plasma accelerator. A means to determine the field strength of the electric/magnetic fields generated when a laser is incident on an object of interest is also outlined. Broad radiography results are reported and future plans for the diagnostic technique are outlined.

INTRODUCTION

Electron radiography (eRad) is a proven, highly penetrative radiography technique that has typically been performed with traditional linear accelerators (LINACs) [1, 2]. Recent work has extended electron radiography techniques into the laser-plasma acceleration (LPA) regime [3, 4] with an emphasis on the radiography of laser-driven dynamics systems.

To compare LPA eRad to traditional LINAC eRad and other radiography methods, the resolution and transmission of said source must be determined. In addition, LPA-based eRad can modify the properties of the object being radiographed via laser-generated plasma if the drive laser is not dumped [4]. Here we present analysis methods to determine the resolution for LPA eRad which include accounting for image distortion caused by the drive laser.

EXPERIMENTAL DETAILS

A polychromatic electron beam generated via LPA with an average energy of ~20 MeV and a bunch charge of up to 700 nC was used to radiograph test objects constructed with varying materials, thicknesses, and feature sizes to fully evaluate the potential of LPA eRad on this platform [4, 5]. Contact radiography was performed on Al, stainless

steel, Cu, Sn and W objects as shown in Figs. 1(a) and 1(b). Projection radiography was performed on solution cast polystyrene, Al, Cu and W objects as shown in Figs. 1(c) and 1(d). All radiographs were taken using MS image plates with 12.5 μm of aluminum in front to dump the laser. MeV-scale electrons have been found to have a relatively flat energy response in image plates and are detected at high efficiency [6]. On each shot, the image plates are saturated by the electron signal. Subsequently, they are scanned repeatedly until saturation no longer exists, and the final, unsaturated scans are used for analysis. Typical scan parameters are sensitivity of 1000 and resolution starting at 100 μm for speed and ending at 25 μm for the final scans in the series.

It should be noted that the majority of the LPA drive laser is transmitted through the LPA plasma source. In the projected configuration, Figs. 1(c) and 1(d), that laser impacts the front face of the projection radiography object with ~10¹⁵ W/cm² intensity and ~20 to 100 joules of laser energy depending on drive specifics. This excess laser energy will impact the target ~100 fs before the electron beam arrives and will generate plasma on the front surface of the object [4]. Consequently, even these supposedly “static” radiography objects were, in reality, laser-ablated dynamic radiography objects.

RADIOGRAPHY ANALYSIS METHOD

Images were then analysed via the software ImageJ [7] and the final scans were grayscale balanced to make the clearest images.

Contact Radiography Resolution

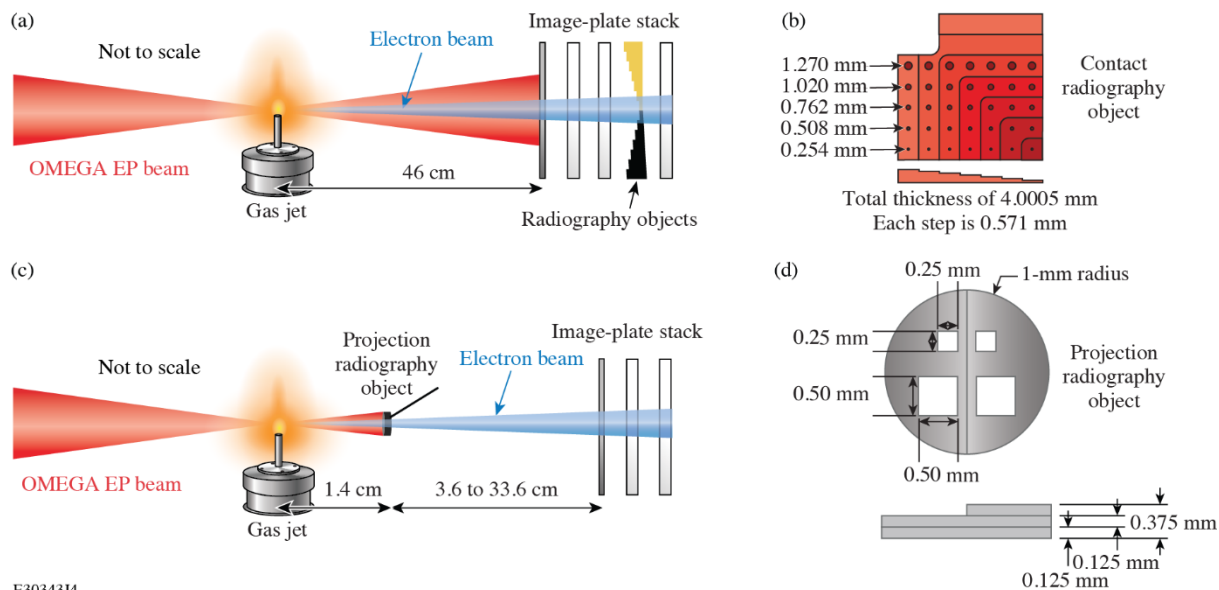
Contact radiography provides the ability to remove the transverse structure of the electron beam using the image plate placed in front of the radiography object as seen in Fig. 2 to record the beam transverse structure before the beam passes through the radiography object. Transverse structure from the beam adds additional blurring to the radiograph that can be eliminated via image division using the software ImageJ [7].

Using these adjusted images, image resolution was determined by creating a box lineout tens of pixels wide across the edges generated by the thickness steps in the radiography object, see Fig. 3(a), and across the edges of the holes in each thickness step. An error function of the form shown in Eq. (1) was then fitted to the lineout as shown in Fig. 3(b).

* This material is based upon work supported by the Department of Energy National Nuclear Security Administration under Award Number DE-NA0003856, the U.S. Department of Energy under Awards DE-SC00215057, the University of Rochester, and the New York State Energy Research and Development Authority.

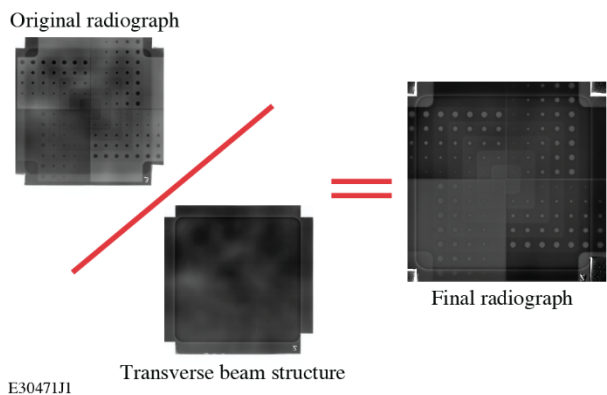
This report was prepared as an account of work sponsored by an agency of the U.S. Government. Neither the U.S. Government nor any agency thereof, nor any of their employees, makes any warranty, express or implied, or assumes any legal liability or responsibility for the accuracy, completeness, or usefulness of any information, apparatus, product, or process disclosed, or represents that its use would not infringe privately owned rights. Reference herein to any specific commercial product, process, or service by trade name, trademark, manufacturer, or otherwise does not necessarily constitute or imply its endorsement, recommendation, or favoring by the U.S. Government or any agency thereof. The views and opinions of authors expressed herein do not necessarily state or reflect those of the U.S. Government or any agency thereof.

[†] gbru@lle.rochester.edu



E30343J4

Figure 1: Experimental setup for (a) contact LPA eRad using radiography test objects placed directly onto image plates and (c) projection LPA eRad using test objects offset from the image plates. Dimensions for (b) contact and (d) projection radiography targets.



E30471J1

Figure 2: Example of background subtraction in contact radiography LPA driven eRad.

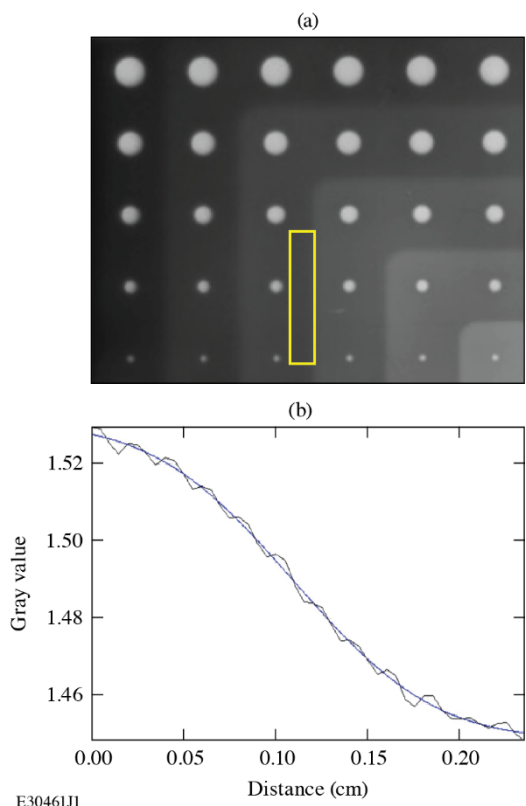
$$y = a + b \operatorname{erf}\left(\frac{x-c}{d}\right) \quad (1)$$

variables a , b , c , and d are fitting parameters for the error function with d giving the resolution.

This procedure was repeated across all edges of holes, all edges of the object and all thickness steps on the object. The results were then averaged for each thickness of material to produce a final resolution at each thickness of material. This total resolution procedure was then repeated for each material tested. Resolutions varied from $<50 \mu\text{m}$ at the thinnest portions of copper and aluminum radiography objects up to $\sim 350 \mu\text{m}$ at the thickest portions of tungsten radiography objects [4].

Projection Radiography Resolution

Projection radiography is the actual use case of interest for eRad, but comes with significant challenges in image



E30461J1

Figure 3: (a) Example of a resolution measurement across thickness step edge for tungsten contact radiography object. The yellow box across the thickness step edge shows the outline of the data used to make the measurement. (b) Lineout of boxed region from (a) (black curve) and error function fit (blue curve).

generation and analysis. There is no easy way to place an image plate between the electron beam and radiography object, so background subtraction is not possible. The long drift distance limits the total imaging resolution possible because of increased scatter-induced blurring [4] which could be compensated with collimators and magnetic optics in future work.

To determine the resolution in projection radiography, the final image plate scan is taken and grayscale balanced for maximum clarity. Box lineouts tens of pixels wide are then taken across the central step in object thickness as well as the object outer edges and hole edges. An error function is fitted to the lineouts and the resolution taken from that function as shown in Fig. 4.

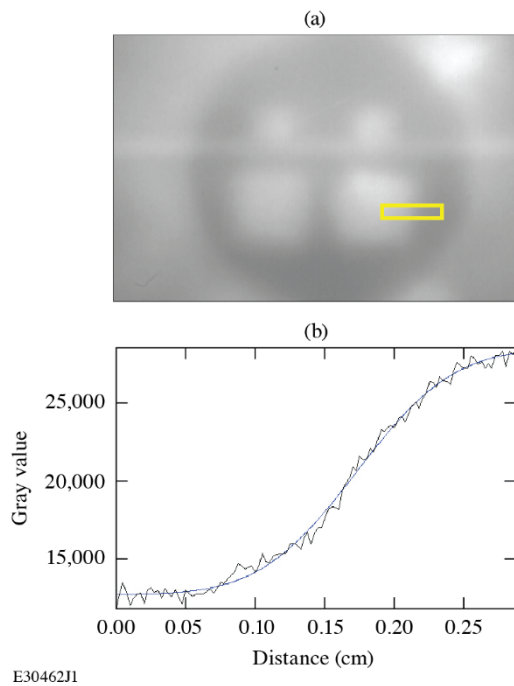


Figure 4: (a) Example of a resolution measurement across a hole for tungsten projection radiography object. The yellow box across the thickness step edge shows the outline of the data used to make the measurement. (b) Lineout of boxed region from (a) (black curve) and error function fit (blue curve).

These measurements are performed multiple times around the resolution measurement point of interest (i.e., an edge or a step in material thickness) and then averaged to determine a final value. Resolutions of the order of 100 μm were seen with this technique [4].

Field Strength Measurement

Plasma-generated electric fields in laser-ablated targets can be roughly measured by measuring the size of features in the eRad image and estimating the field strength needed to produce those features. When measuring the sizes of the static projection radiography objects shown in Fig. 1(d), it was noticed that the resulting radiographs were $\sim 1.5\times$ smaller than expected as illustrated in Fig. 5.

Previous data suggests that this size discrepancy was caused by plasma-generated electric fields acting like an electrostatic lens on the electron beam [8]. Using the average electron beam energy of ~ 20 MeV [5], it was determined that the electric field corresponded to ~ 1 GV/m [4] would generate the magnification discrepancies seen. This is well in line with previous laser-plasma electric field strengths at this laser intensity [8].

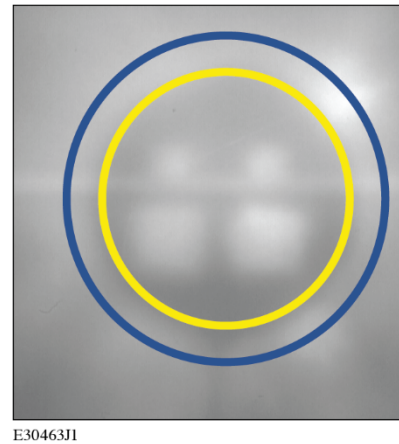


Figure 5: Projected radiograph of tungsten radiography object showing the size discrepancy caused by the plasma electric field focusing of the electron beam. Blue outline shows the expected image size of ~ 1.8 cm if there was no plasma focusing, and the yellow circle shows the measured diameter of ~ 1.2 cm.

CONCLUSION

Analysis methods for LPA-generated eRad are presented for determining radiography resolution in both contact and projection radiography configurations. These methods account for transverse beam structure in contact radiography, but not projection radiography. A method of determining plasma-generated field strength in laser-ablated radiography objects using distortions in LPA-generated eRad is also outlined. Future work will seek to use these techniques to radiograph laser-ablated objects of interest to the high-energy-density-physics community and add magnetic optics to improve imaging resolution.

REFERENCES

- [1] F. Merrill *et al.*, “Electron radiography,” *Nucl. Instrum. Methods Phys. Res. B*, vol. 261, no. 1–2, pp. 382–386, 2007. doi:10.1016/j.nimb.2007.04.127
- [2] F. E. Merrill *et al.*, “Demonstration of transmission high energy electron microscopy,” *Appl. Phys. Lett.*, vol. 112, no. 14, p. 144103, 2018. doi:10.1063/1.5011198
- [3] W. Schumaker *et al.*, “Ultrafast electron radiography of magnetic fields in high-intensity laser-solid interactions,” *Phys. Rev. Lett.*, vol. 110, no. 1, p. 015003, 2013. doi:10.1103/PhysRevLett.110.015003
- [4] G. Bruhaug *et al.*, “Single shot electron radiography using an LPA driven by a kilojoule-class picosecond laser,” submitted to Scientific Reports.

- [5] J. L. Shaw *et al.*, “Microcoulomb ($0.7 \pm 0.4/0.2 \mu\text{C}$) laser plasma accelerator on OMEGA ep,” *Sci. Rep.*, vol. 11, no. 1, p. 7498, 2021. doi:10.1038/s41598-021-86523-5
- [6] G. Boutoux *et al.*, “Study of imaging plate detector sensitivity to 5–18 MeV electrons,” *Rev. Sci. Instrum.*, vol. 86, no. 11, p. 113304, 2015. doi:10.1063/1.4936141
- [7] C. A. Schneider, W. S. Rasband, and K.W. Eliceiri, “NIH image to ImageJ: 25 years of image analysis,” *Nat. Methods*, vol. 9, no. 7, pp. 671–675, 2012. doi:10.1038/nmeth.2089
- [8] J. L. Dubois *et al.*, “Target charging in short-pulse-laser-plasma experiments,” *Phys. Rev. E*, vol. 89, no. 1, p. 013102, 2014. doi:10.1103/PhysRevE.89.013102